Thermal and Wind Effects on the Azimuth Axis Tilt of the ASTE 10-m Antenna

Nobuharu UKITA, Hajime EZAWA, Bungo IKENOUE, and Masao SAITO

Abstract

The azimuth axis tilt of the ASTE 10-m antenna induced by thermal and wind loadings was investigated with a dual-axis inclinometer on the azimuth axis, along with thermometers on the pedestal and yoke structures and an ultrasonic anemometer on a nearby weather station. The dependences of the inclinometer zero-point offsets against temperature of the device, temperature gradients in the pedestal and yoke structure were obtained for the measurements over 11 months during the antenna being parked at its home position (azimuth angles = ± 180 degrees, an elevation angle = 60 degrees) under wind velocities < 8 m s^{-1}. The temperature dependences of the zero-point offsets were found to be 1.24 and -0.46 arcseconds/degree, and were close to those obtained with an independent method. The azimuth axis tilts due to the temperature difference between the two opposite sides of pedestal walls were found to be about 1.1 and 1.7 arcseconds/degree, and consistent with 1.5 arcseconds/degree estimated with a simple model. The residual axis tilt of the whole samples after removal of the temperature dependences shows dependence against overturning moment estimated from the wind data. The stiffness of the antenna structures between the yoke base section and the ground was estimated to be 5.3 and 3.4 GNm/rad using the observed tilts in two directions; and were smaller than 6.0 GNm/rad from a mechanical model prediction. Based on these field experiments, we discuss the improvements and limitations of pointing performance with the inclinometer metrology system.

1. Introduction

Pointing accuracy of a radio telescope is one of key performances that determine the quality and throughput of data, which in the end influences research productivity of the telescope. It is desirable that blind pointing errors on the whole sky do not exceed about one fourth of a telescope beamwidth for pointing checks/corrections prior to observations, and that tracking errors are less than one tenth of the beamwidth to keep a sensitivity loss within 3 percents for a compact object for an hour or two. The 10-m antenna of the Atacama Sub-millimeter Telescope Experiment (ASTE) project of Nobeyama Radio Observatory* is an experimental telescope for sub-millimeter observations (Ukita et al., 2000; Ezawa et al., 2004) at a windy site. Because the antenna is exposed to wind and sunshine, it is a tough task to achieve pointing performance requested for the antenna whose beamwidth is 7 arcseconds at 950 GHz.

There are two types of pointing errors, repeatable and non-repeatable errors. The repeatable errors include mechan-

---

ical misalignments and gravity deformation that can be corrected with a simple pointing model with 8 to 20 terms (e.g., Greve et al., 1996; Ukita, 1999; Ukita et al., 2004; Mangum et al., 2006). Errors due to friction, servo errors in drive systems, and rapidly changing wind turbulence are non-repeatable. Pointing errors due to thermal and static wind loadings are in-between. Thermal deformations are, in principle, predictable from temperature measurements of the antenna structure with the aid of finite element model (FEM) calculations (e.g., Bremer and Peñalver, 2002). The static wind effects can also be estimated using coefficients derived from wind tunnel and/or field experiments. These two effects are slow in time and can also be corrected with a telescope control computer.

The structure surface of the ASTE antenna is protected with thermal insulation boards to minimize the thermal deformation. There will be, however, inevitable thermal effects on the antenna structure. For example, a tilt of a steel square box amounts to 2.3 arcseconds when it has temperature gradient of one degree across the two opposite sides of its walls. Drag force of head wind of 20 m s^{-1} on a 10-m dish is about 17 kN at the site. It is estimated that this loading on the ASTE antenna (113 kNm) makes the yoke base structure, the azimuth bearing structure, the antenna pedestal, fastener bolts, and the concrete foundation bent by a total of about 4

arcseconds. These estimates clearly suggest that we need metrology systems to cope with the inevitable deformations of the antenna mount structure. Many telescopes have used high precision inclinometer(s) as a metrology device for improvements of pointing performance (e.g., Kibrick et al., 1998; Ukita 1999; Peñalver et al., 2000; Parker and Srikanth, 2001, Prestage et al., 2004). The ASTE antenna also has a dual-axis inclinometer on the azimuth axis to measure the axis tilt and correct the pointing offsets accordingly in real-time (Ukita et al. 2000).

This report describes one of such metrology systems to achieve the ultimate goal of the pointing performance of the ASTE 10-m telescope. We investigate whether the incli-nometer consistently detects the azimuth axis tilts induced by thermal loads measured in the field, and whether it has long term stability good enough for our pointing goal. We also look into wind load effects on the mount structure. Section 2 describes our experiment system and measurement data for a year. Section 3 shows our analyses of both thermal and wind loading deformations. Section 4 discusses pointing performance improvements by the inclinometer metrology system and its limitation.

2. Equipment

The ASTE 10-m antenna has an alt-azimuth mount. Figure 1 displays its steel mount structure; its pedestal has an average diameter of 2.7 m and a height of 1.8 m and the ele-vation axis is supported by its yoke arms at a height of 6.5 m from the ground. The antenna is located at Pampa la Bola (23 deg south, 4h30m east, and altitude 4,800 m) in Atacama
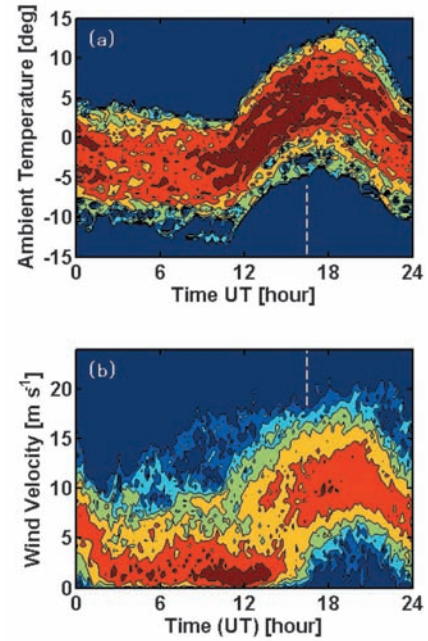
Figure 2. Diurnal variations of ambient temperature (upper) and wind velocity (lower) measured from February to December, 2005. The white dashed lines indicate local noon. The antenna location is 23 deg south, 4h30m east.

desert, northern Chile. Figure 2 shows diurnal variations of ambient temperature and wind velocity. During night the ambient temperature is stable and wind velocity is low (a typical mean velocity of 4.5 m s^{-1}), and during daytime tem-perature changes are large and wind velocity is high (typical mean velocities >10 m s^{-1} in the afternoon). A prevailing wind direction is west, and a mean air pressure is 570 hPa.

We used a dual-axis inclinometer (Nivel20, Leica) with a digital output port (RS232C). It incorporates a fluid mirror and a position sensitive diode to measure tilts in two axes. It
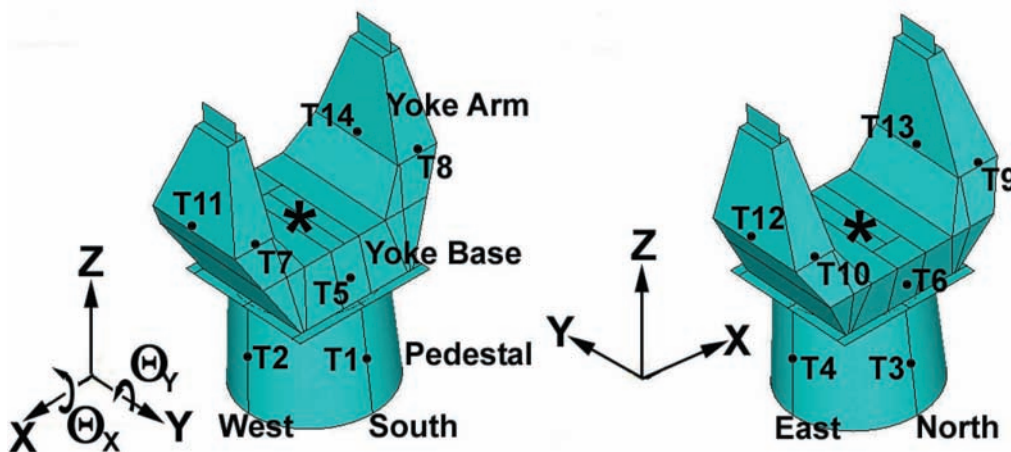
Figure.1 The pedestal and yoke structure of the ASTE 10-m antenna. Star marks are the location of the inclinometer, dots indicate the temper-ature sensors that are installed on inner surfaces of the structure. The antenna is at Az = ± 180 degrees (South). The coordinate system used in this report is also shown.

provides a resolution of 0.001 mrad (0.2 arcseconds) and a dynamic range of ± 1.5 mrad (± 5 arcminutes). It has an output time constant of about 1 second. The data are logged every second. It is located on the azimuth axis in the yoke structure (see figure 1) to avoid the centrifugal force of the antenna azimuth movement. Its zero-point offsets vary with the device temperature. According a specification sheet, they shall be less than 0.005 mrad/degree (1 arcsecond/degree). They can be measured from the average of readouts during a full turn of 360 degrees in azimuth. Their temperature dependences can be determined from a series of such measurements at different device temperatures (e.g., Ikenoue et al., 2005). They are 1.29 ± 0.15 arcseconds/degree in Θ_x and -0.29 ± 0.09 arcseconds/degree in Θ_y (see Appendix).
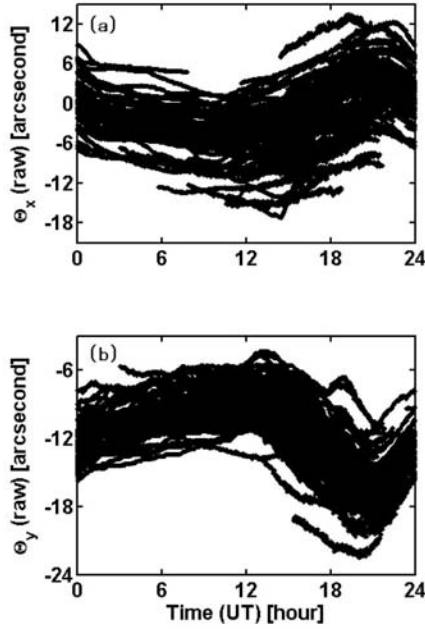
Figure 3. Diurnal variations of tilts (upper: in Θ_x; lower: Θ_y) measured from February to December, 2005. The antenna was at its home position of Az = ± 180 deg. and El = 60 deg.

The ASTE antenna has about 170 thermocouple thermometers (T-type) on its antenna structure, and 14 of them at the pedestal and yoke structure (see figure 1). The outputs from the thermometers have been recorded at 3-minutes intervals through a data logger (THERMODAC-6, Etodenki Co., Ltd) with a resolution of 0.1 degrees.

A 2D ultrasonic anemometer (WindObserver II, Gill Instruments Ltd) is installed atop of a weather tower at a height of 6 m, comparable to that of the elevation axis of the antenna. The tower is located in the SW direction (Az = -134 deg.) and at 35 m from the antenna. The data are logged at 4 Hz.

3. Analysis

The data we handled in this report are those logged when the antenna was parked at its home position angle of Az = ± 180 and El = 60 degrees for intervals longer than six hours. There were 101 such occasions in the period from February to December, 2005. To reduce data samples, we averaged the data from the inclinometer and anemometer for one minute, which resulted in 92,000 samples. The thermometer data were interpolated for each sample point. In figure 3, the measured individual tilts are plotted as dots to show diurnal variations. Typical amplitudes of the diurnal variations in Θ_x and Θ_y are 10 and 6 arcseconds, respectively. It seems that they can be interpreted in terms of the zero-point offset variations and temperature gradients in the antenna structure, based on the pre-considerations and data-inspections mentioned in sections 1 and 2.

In addition, it should be noticed that in figure 3 there are both thin and burred traces in time, which seems to be an indication of a wind effect. Therefore we temporally set a wind velocity threshold of 8 m s^{-1} in the following thermal effect study, which results in about 54,000 samples. This threshold value is a compromise to have a certain high number density of sample points in daytime where temperature variations are large and to minimize the wind load effects.

3.1 Thermal Effects

By the above selection of the antenna position and wind velocity, it is now possible to make a simple model to describe the azimuth axis tilts. We use following empirical equations:

$$\Theta_x = C_1 T_0 + C_2 \Delta T_{S-N} + C_3 \Delta T_{F-R} + C_4 , \qquad (1)$$

and

$$\Theta_y = C_5 T_0 + C_6 \Delta T_{E-W} + C_7 \Delta T_{R-L} + C_8 , \qquad (2)$$

where T_0 is the inclinometer temperature, $\Delta T_{S-N} (= T_1 - T_3)$ and $\Delta T_{E-W} (= T_4 - T_2)$ are temperature gradients of the pedestal structure, $\Delta T_{F-R} (= T_5 - T_6)$ and $\Delta T_{R-L} (= T_{14} - T_{13})$ are temperature gradients in the yoke structure.

We have recognized an additional problem. The inclinometer outputs jump in a discontinuous manner when changing from an active drive state by the electronic controlled drive motors to a parking state engaged by mechanical brakes. The jumps are typically a few arcseconds and non-repeatable. Therefore we take the difference approach of data analysis for these equations. We search for epochs at which the wind velocity is a minimum in individual data sets. Figures 4 and 5 display these difference values thus
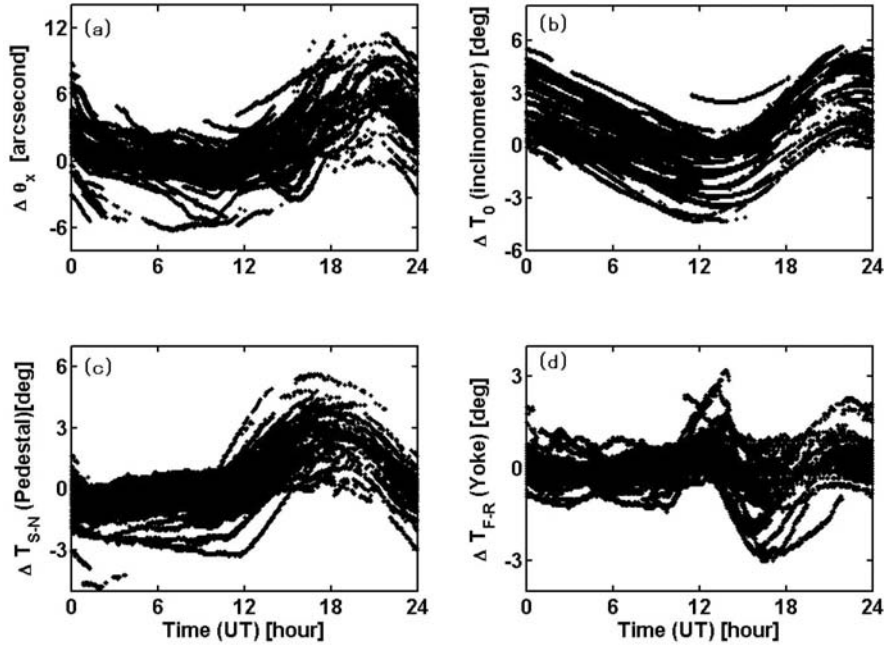
Figure 4. (a) Elevation tilts ($\Delta\Theta_x$) corrected for tilt jumps due to brake operation of the drive motors (see the text); (b) the inclinometer temperature (T_0); (c) temperature difference between front- and rear-side of the pedestal ($T_1 - T_3$); (d) temperature difference between front- and rear-side of the yoke base ($T_5 - T_6$) for the antenna position of Az = ± 180 *and* El = 60 degrees and wind velocities < 8 m s^{-1}. Note that the vertical scales are different among the panels.

obtained for the tilt, the inclinometer temperature, and the temperature gradients in the pedestal and yoke structures.

The inclinometer temperature variations are smooth (figures 4b and 5b), and have large time lags with respect to the ambient temperature (figure 2a). The amplitudes are typically 5 degrees. The east-west temperature gradient variations in the pedestal clearly show the effect of sunlight,

namely about 1 degree in the morning and about –1 degree in the evening (figure 5c). On the contrary, the south-north temperature gradient variations (figure 4c) show large amplitudes of about 3 degrees and mimic the ambient temperature variations. This is because the southern part of the pedestal has the azimuth gear boxes and its surface is not protected by insulator boards. The temperature of this part follows closely
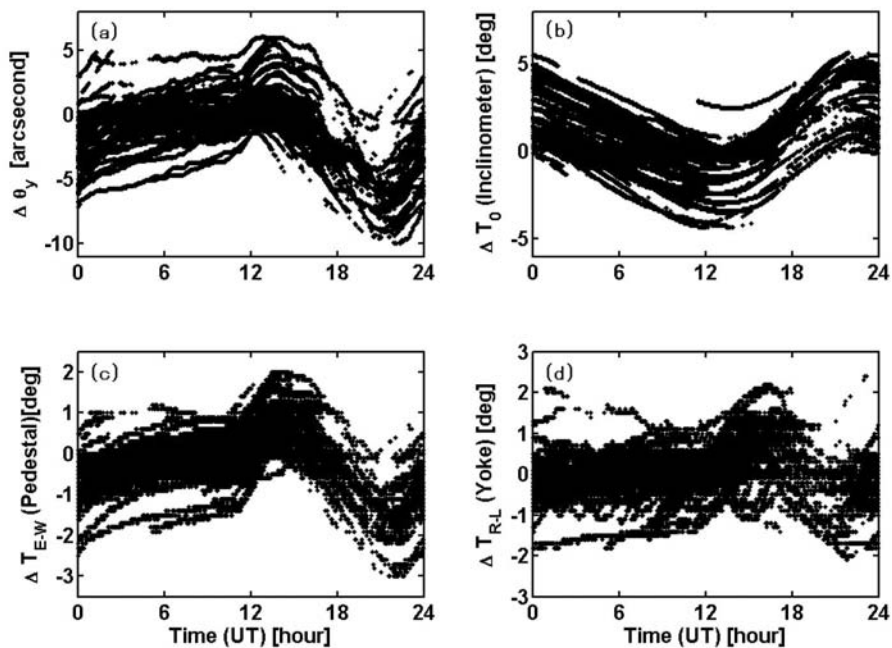

Figure 5. Same as figure 4, but for (a) cross-elevation tilts ($\Delta\Theta_y$); (c) temperature difference between east- and west-side of the pedestal ($T_4 - T_2$); (d) temperature difference between right- and left-side of the yoke ($T_{14} - T_{13}$).

Table 1. Temperature dependence of tilt.

Item	Inclinometer	Pedestal		Yoke		Note
Variables	T_0	ΔT_{E-W}	ΔT_{S-N}	ΔT_{R-L}	ΔT_{F-R}	
unit	["/deg]	["/deg]	["/deg]	["/deg]	["/deg]	
Θ_x	1.24±0.02	....	1.07±0.04	....	1.54±0.03	Fig. 4
Θ_y	−0.46±0.05	1.73±0.23	...	0.40±0.10	...	Fig. 5

the ambient temperature. Figure 4d shows the front-rear temperature gradient variations of the yoke, which is also the effect of sunlight, namely about –2 degrees near noon.

We have made least squares fits for the differential tilts, and have obtained coefficients for these variables (table 1). The uncertainties of coefficients have been estimated from the cases of wind velocity thresholds of 7 and 9 m s^{-1}. The temperature dependences of inclinometer zero-point offsets in Θ_x, C_1=1.24 ± 0.02 arcseconds/degree, and in Θ_y, C_5= –0.46 ± 0.05 arcseconds/degree are close to 1.29 ± 0.15 and –0.25 ± 0.09 arcseconds/degree, respectively, obtained from the independent method. The azimuth axis tilt due to the temperature difference between the two opposite sides of pedestal walls is estimated to be about 1.5 arcseconds/degree with a simple model. The observed coefficients were 1.07 and 1.73 arcseconds/degree.
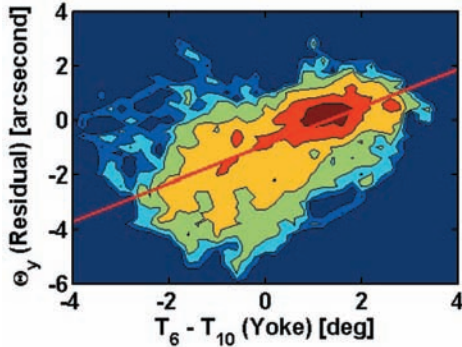
Figure 6. Residual tilts in Θ_y after the adjustments of azimuth tilt jumps by brake operations against temperature gradient in the yoke structure, $\Delta T_{6-10} = T_6 - T_{10}$ (see the text). The thin line shows a linear fit.

The tilts of the yoke structure show complex behaviours. After the corrections with the coefficients in table 1 and the adjustments of offsets due to the jumps of brake operations, which will be described in section 3.2, we have searched for additional correlations between the residual tilts in Θ_x and Θ_y and differences among temperatures at the 14 locations for the entire data samples. There have been found no significant correlations in the Θ_x. We have, however, found a correlation between the residual tilts in Θ_y and the difference between the rear face of the yoke base, T_6, and the rear face of right yoke arm, T_{10} (figure 6). A possible reason is the following. The asymmetric layout of a rear platform

for instrument boxes which make shadows on the left half of the rear faces of the yoke, which in turn produces a temperature gradient along the elevation axis direction during daytime. Because in the first step of our analysis the samples mostly consist of those during night (low wind velocities), this thermal effect due to the sunlight does not appear clearly.

The coefficient for the front-rear temperature gradient in the yoke structure, C_3, was 1.54 arcseconds/degree (table 1), and is larger than that estimated from a simple model (1.0 arcseconds/degree). These suggest that the yoke structure has a scale length of temperature gradient shorter than the distances between the sensors. We need more thermometers to reveal temperature distributions in the yoke structure. Therefore it might to be not useful to make comparisons of the coefficients from the measurements and simple models that assume a linear gradient across the structures.

3.2 Wind Effect

Wind loads on a parabola dish can be estimated using the table of force coefficients obtained from wind tunnel experiments (Levy, 1996). The *f/D* ratios of the dish used in the tunnel experiments and of the ASTE antenna are 0.33 and 0.35, respectively; and close each other. We have to notice, however, the shape difference between a thin parabola of the model (like a satellite antenna for home use) and the ASTE main dish. The back-up structure of the ASTE main dish has a thickness of 1.8 m at its center, comparable to the depth of front surface profile of the reflector; in other words the projected area viewed from its side is twice that of a thin parabola. We used the side force coefficients modified accordingly. For a receiver cabin we simply assumed that C_d is 2 (Simiu and Scanlan, 1996). Table 2 gives overturning moments by wind of 10 m s^{-1} on the ASTE antenna for 13 directions. We can estimate the stiffness of the antenna mount by comparing observed tilts with wind loads calculated with table 2. We use following empirical equations:

$$\Theta_x = C_9 M_x + C_{10} , \qquad (3)$$

and

$$\Theta_y = C_{11} M_y + C_{12} , \qquad (4)$$

where M_x and M_y are overturning moments.

Table 2. Overturning moment by wind of 10 m s^{-1}.

Overturning	Wind Direction [deg]												
Moment	-180	-165	-150	-135	-120	-105	-90	-75	-60	-45	-30	-15	0
M_x [kNm]	24	21	23	20	13	7	0	-7	-9	-11	-16	-15	-14
M_y [kNm]	0	-1	-2	-5	-9	-11	-13	-12	-10	-8	-6	-3	0

We have encountered again the problem of the inclinometer output jumps due to brake operation. In order to estimate the jumps of the individual data sets, we have made least squares fits to each data set with equations 3 and 4 to find constants of C_{10} and C_{12}. These constants were subtracted from the individual data sets. Figures 7a and c display the tilts of all the 92,000 samples after the corrections of thermal effects and these offset jump adjustments.

Figures 7b and d show the tilts against the overturning moments by wind. We have made least squares fits to the whole samples. The inverse of C_9 and C_{11} give the stiffness of the antenna structures between the yoke base section and the ground. They are 5.3 ± 0.3 and 3.4 ± 0.1 GNm/rad in the two directions parallel and perpendicular to the elevation axis, respectively. These values are smaller than 6.0 GNm/rad from a model calculation. Angles of bend by a loading of 113 kNm on the yoke base, the azimuth bearing, the antenna pedestal, fastener bolts, and the concrete foundation are 0.2, 2.1, 0.7, 0.8, and <0.1, respectively; and a total of about 4 arcseconds.

3.3 Contents of Tilt Variations

In summary we have untangled the observed inclinometer outputs with six terms of sources. The large variations and scatters seen in figures 3a and b are reduced those shown in figures 7a and c after the removal of the thermal loading and brake operation effects, and to the final unknown residuals shown in figure 8a and b after the elimination of the wind loading effect. We have calculated their standard deviations and listed in the second and last columns of table 3. We have evaluated them in the time ranges from UT=3h to 9h (night) and from UT=15h to 21h (daytime). We have also calculated standard deviations for the individual sources of variations (from the third to 8th columns of table 3). The biggest contributor was the temperature variation of the inclinometer itself. The second was the jumps due to brake operation, which is not relevant to the observing performance. The third was the tilt in Θ_x due to the temperature gradient between the front- and rear faces of the yoke base.
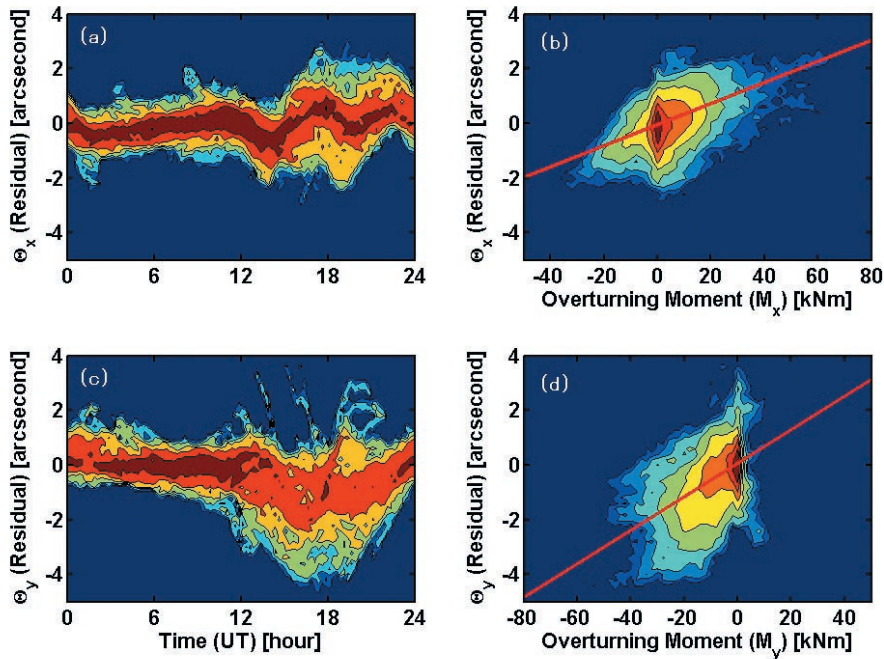
Figure 7. Residual tilts in Θ_x and Θ_y (a, c) and their dependences against wind loads M_x and M_y, respectively (b, d). The thin lines show linear fits.

Table 3. Contents of tilt variations.

	Total (raw)	Thermal Tiltmeter	Thermal Pedestal	Thermal Yoke I	Thermal Yoke II	Wind	Brake Operation	Residual Unknown
$\sigma(\Theta_x)$ (night)	3.3	3.7	0.6	0.8	...	0.1	2.1	0.4
(daytime)	5.0	4.0	0.8	1.6	...	0.4	...	0.8
$\sigma(\Theta_y)$ (night)	1.8	1.4	0.5	0.2	0.4	0.3	0.6	0.5
(daytime)	3.1	1.5	1.3	0.2	0.6	0.6	...	1.1
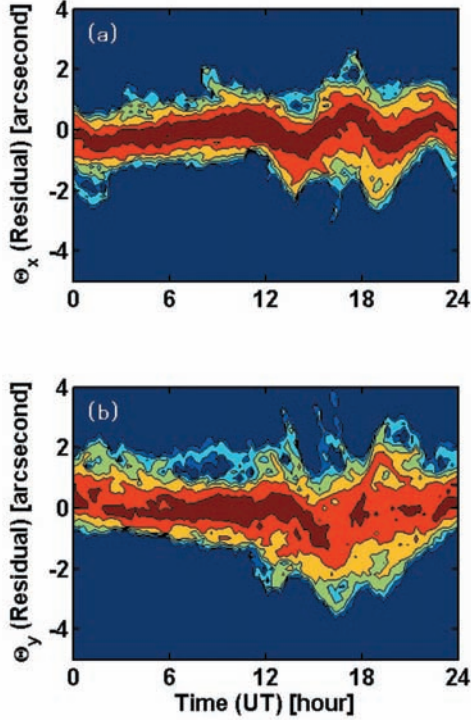
Figure 8. Residual tilts in Θ_x and Θ_y after corrections of wind load effects.

4. Discussion

Our inclinometer is a key metrology device for the antenna pointing performance. Our analysis in the previous section seems to suggest that the inclinometer fairly consistently detects the azimuth axis tilts and that it has long term stability far better than 1 arcsecond (figure 8). These results are encouraging and clearly deserve further studies in detail in the following pages.

Ironically, most of the variations were induced by the inclinometer temperature variation. One may propose to keep the temperature of inclinometer constant with an additional device(s) (e.g., a controller with heater). Such active approach might produce a thermal deformation of the structure near the inclinometer and it is no longer the reference plane for the inclinometer. Our passive approach is to leave it in a simple temperature distribution and to minimize local deformations. The ASTE antenna has no heat sources such as electric devices inside the pedestal and yoke structures, except the azimuth angle encoder and the inclinometer. This is one of our antenna design concepts as an experimental telescope. The motivation of this report is based on this approach. Therefore it is essential to calibrate the device accurately.

We estimate a required calibration accuracy from our field data. The standard deviation of the inclinometer temperatures during the 11 months was 3.5 degrees. If we temporally assume that the error allocated in a blind pointing error budget for the inclinometer itself to be 0.5 arcseconds, the calibration accuracy should be about 10 %, namely 0.5 arcseconds divided by the coefficient of 1.24 arcseconds/degree and by 3.5 degrees. The typical slope of inclinometer temperature variation in figure 4b was 0.67 degrees/hour. If we assume that the error allocated in a tracking error budget for the inclinometer itself to be 0.2 arcseconds, which is equal to the inclinometer output resolution, the calibration accuracy should be again about 10 %, namely 0.2 arcseconds divided by the coefficient of 1.24 arcseconds/degree, by the temperature slope of 0.67 degrees/hour, and by 2 hours of tracking time span. Since the discrepancy

Table 4. Improvement and limitation of pointing performance with the inclinometer system.

	Improvement Thermal Pedestal	Improvement Thermal Yoke	Improvement Thermal Sub-total	Wind	Total	False Correction
$\sigma(\Theta(\text{All} - \text{sky})_{\text{radial}})$ (night)	0.7	0.9	1.2	0.2	1.2	0.6
(daytime)	1.4	1.8	2.5	0.6	2.8	1.2
$\sigma(\Theta(\text{Tracking})_{\text{radial}})$ (night)	0.15	0.16	0.23	0.09	0.25	0.20
(daytime)	0.43	0.31	0.56	0.32	0.68	0.50

between our two measurements with the independent methods was within 10 %, we conclude that the required calibration accuracy has been achieved.

The following three paragraphs discuss the improvement and limitation of pointing performance with the current inclinometer metrology system. The inclinometer detects both a large scale and local deformations below the yoke base structure, namely in the yoke base itself, azimuth bearing, pedestal and concrete foundation. One of the key roles of the inclinometer is to eliminate effects due to mechanical deformations of the azimuth bearing, such as its non-repeatable runout, that cannot be described with a simple pointing model. Aside this, we look into the advantages and disadvantages of the inclinometer system. The advantage is, of course, to detect a tilt in a large scale, namely the azimuth axis tilt. The disadvantage is that if there are local deformations in the yoke base irrelevant to the true axis tilt, the metrology system makes a false correction of pointing.

Here we assume that in our experiments the true axis tilts are those detected with linear fits in table 3 (fourth to seventh columns), and the false tilts are the residuals in figure 8a and b (the last column of table 3). We have calculated standard deviations of improvements and false corrections for the all-sky pointing and 2-hours tracking (table 4). We have evaluated them in the time ranges from UT=3h to 9h (night) and from UT=15h to 21h (daytime) and for the case of an elevation angle of 60 degrees. Table 4 shows that the system gives improvements in the all-sky pointing operations, but no significant net-improvements in the 2-hours tracking. If we assume that the error allocated in a blind pointing error budget and the error allocated in a tracking error budget for the false correction to be 0.5 and 0.2 arcseconds, respectively, the current system meets this requirement during night but not during daytime. These investigations suggest that we need a countermeasure against the local temperature irregularity in the yoke base to achieve the pointing performance imposed on the ASTE antenna.

Although we have discussed only the deformations between the yoke base and the ground, we should notice that it is essential to estimate the angular position of the elevation axis. The relative angular position between the elevation axis and the inclinometer should be found with an accuracy necessary as the metrology system. Not only local deformation near the inclinometer but also deformations of the two yoke arms should be estimated with high accuracy with a high number density of sensors. Therefore we have recently installed about 80 additional thermometers in the yoke arm and base structures as a new step to achieve its ultimate

pointing goal.

Finally we discuss about the wind load. The measured stiffness was smaller than the model prediction. It is difficult to estimate the uncertainties of force coefficients (Levy, 1996), and it seems that we should be satisfied with our results within a discrepancy factor of 2. It is highly desirable that we make dedicated experiments with an additional device(s) under a specific condition to make it clear what is the source of this discrepancy. A proper antenna-wind configuration is an attack angle of zero degree, e.g., when the wind direction is –90 degree, the antenna is at Az = –90 deg. and El = 0 deg. Because the configuration is simple and there have been a number of tunnel experiments, the coefficients for this configuration are most reliable. Possible locations of the additional inclinometer(s) are on the concrete foundation and beneath the azimuth bearing.

In summary, we have investigated the azimuth axis tilt of the ASTE 10-m antenna induced by thermal and wind loadings with a dual-axis inclinometer. We have interpreted the observed tilts with six terms of sources (table 3). Most of the tilt variations were of thermal origin. We have revealed the tilt due to static wind loadings and derived the stiffness of the antenna mount structure (figure 7). We have discussed the improvements and limitations of pointing performance with the current inclinometer metrology system.

Variation of Inclinometer Zero-Point Offsets

Our dual-axis inclinometer (Nivel20, Leica) has temperature dependences of zero-point offsets against its device temperature. One method to obtain zero-point offsets is our method described in our paper, and another is to measure the average of readouts during a full turn of 360 degrees in azimuth. Their temperature dependences can be determined from a series of measurements at different device temperatures (e.g., Ikenoue et al., 2005). Figure 9 shows such 190 measurements made repeatedly on several days in the period 2004 April 25 to June 9. It takes only 9 minutes for a single measurement. We have made least squares fits, and have obtained coefficients in the following empirical equations:

$$\Theta_x = (1.29 \pm 0.15) \times T_0 + 0.7 \pm 0.4 , \qquad (5)$$

and

$$\Theta_y = (-0.29 \pm 0.09) \times T_0 - 0.0 \pm 0.2 , \qquad (6)$$

where T_0 is the device temperature of the inclinometer. The uncertainties in parameters are given in 3σ.
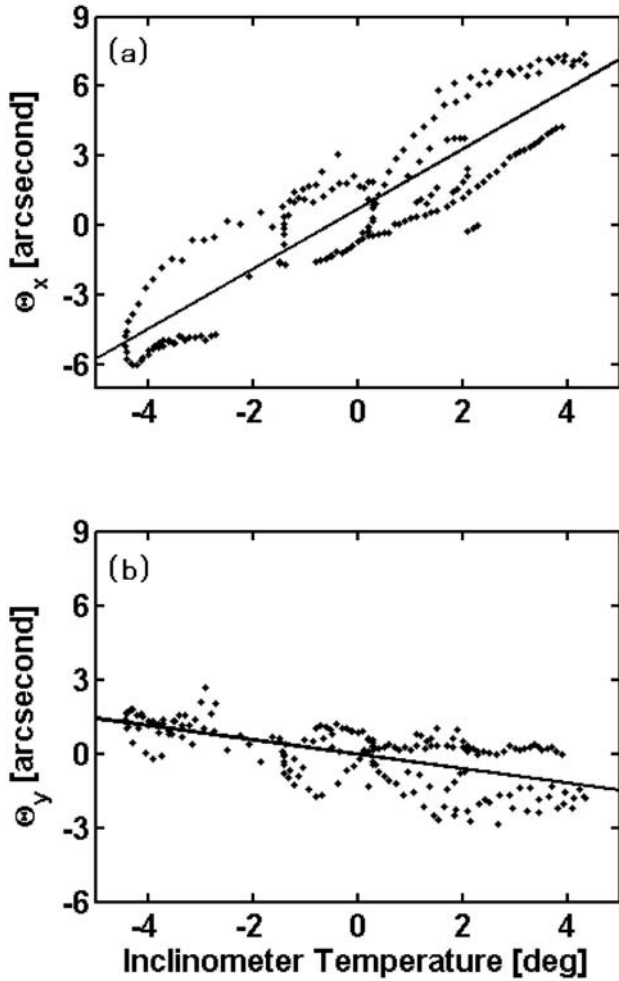

Figure 9. Variations of inclinometer zero-point offsets against its device temperature

References

Bremer, M. and Peñalver, J. 2002, "FE model based interpretation of telescope temperature variations", *Proc. SPIE*, **4757**, 186-195.

Ezawa, H., Kawabe, R., Kohno, K., and Yamamoto, S. 2004, "The Atacama Submillimeter Telescope Experiment (ASTE)", *Proc. SPIE,* **5489**, 763-772.

Greve, A., Panis, J.-F., and Thum, C. 1996, "The Pointing of the IRAM 30-m Telescope", *Astron. Astrophys. Suppl.*, **115**, 379-385.

Ikenoue, B., Ukita, N., Saito, M., Ezawa, H. 2005, "Performance evaluation of an ALMA 12-m prototype antenna with an optical pointing telescope system ", *Report Natl. Astron. Obs. Japan*, **8**, 111-123 (in Japanese).

Kibrick, R.I., Robinson, L.B., Wallace, V., Cowley, D.J. 1998, "Tests of a precision tiltmeter system for measuring telescope position", *Proc. SPIE,* **3351**, 342-353.

Levy, R. 1996, " Structural Engineering of Microwave Antennas", IEEE Press, Piscataway, NJ.

Mangum, J.G., et al. 2006, "Evaluation of ALMA Prototype Antennas", *Publ. Astron. Soc. Pacific*, **118**, 1257-1301.

Parker, D.H., Srikanth, S. 2001, " Measurement system for the Green Bank Telescope", Antennas and Propagation Society International Symposium, 2001. *IEEE*, **4**, 592 - 595.

Peñalver, J., Lisenfeld, U., Mauersberger, R. 2000, "Pointing with the IRAM 30m Telescope", *Proc. SPIE,* **4015**, 632-640.

Prestage, R. M., Constantikes, K. T., Balser, D. S., Condon, J. J. 2004, "The GBT precision telescope control system", *Proc. SPIE,* **5489**, 1029-1040.

Simiu, E. and Scanlan, R.H. 1996, "Wind Effects on Structures", John Wiley & Sons, Inc., Hoboken, NJ.

Ukita, N. 1999, "Thermal Effects on the Pointing of the Nobeyama 45-m Telescope", *Publ. Natl. Astron. Obs. Japan*, **5**, 139-147.

Ukita, N. et. al. 2000, "NRO 10-m submillimeter telescope", *Proc. SPIE,* **4015**, 177-184.

Ukita, N. et. al. 2004, "Design and performance of the ALMA-J prototype antenna", *Proc. SPIE,* **5489**, 1085-1093.